Taylor & Francis
Taylor & Francis Group

RESEARCH PAPER

Pharmacological inactivation of CDK2 inhibits MYC/BCL-XL-driven leukemia in vivo through induction of cellular senescence

Wesam Bazzar[a]*, Matteo Bocci [a†]*, Eduar Hejll[a‡]*, Vedrana Högqvist Tabor[a§], Per Hydbring[a¶], Alf Grandien[b], Mohammad Alzrigat[a], and Lars-Gunnar Larsson [a]

[a]Department of Microbiology, Tumor and Cell Biology (MTC), Karolinska Institutet, Stockholm, Sweden; [b]Center for Hematology and Regenerative Medicine, Department of Medicine, Karolinska University Hospital- Huddinge, Stockholm, Sweden

ABSTRACT

Deregulated expression of the MYC oncogene is a frequent event during tumorigenesis and generally correlates with aggressive disease and poor prognosis. While MYC is a potent inducer of apoptosis, it often suppresses cellular senescence, which together with apoptosis is an important barrier against tumor development. For this latter function, MYC is dependent on cyclin-dependent kinase 2 (CDK2). Here, we utilized a MYC/BCL-X$_L$-driven mouse model of acute myeloblastic leukemia (AML) to investigate whether pharmacological inhibition of CDK2 can inhibit MYC-driven tumorigenesis through induction of senescence. Purified mouse hematopoietic stem cells transduced with MYC and BCL-X$_L$ were transplanted into lethally irradiated mice, leading to the development of massive leukemia and subsequent death 15–17 days after transplantation. Upon disease onset, mice were treated with the selective CDK2 inhibitor CVT2584 or vehicle either by daily intraperitoneal injections or continuous delivery via mini-pumps. CVT2584 treatment delayed disease onset and moderately but significantly improved survival of mice. Flow cytometry revealed a significant decrease in tumor load in the spleen, liver and bone marrow of CVT2584-treated compared to vehicle-treated mice. This was correlated with induced senescence evidenced by reduced cell proliferation, increased senescence-associated β-galactosidase activity and heterochromatin foci, expression of p19^{ARF} and p21^{CIP1}, and reduced phosphorylation (activation) of pRb, while very few apoptotic cells were observed. In addition, phosphorylation of MYC at Ser-62 was decreased. In summary, inhibition of CDK2 delayed MYC/BCL-X$_L$-driven AML linked to senescence induction. Our results suggest that CDK2 is a promising target for pro-senescence cancer therapy, in particular for MYC-driven tumors, including leukemia.

Introduction

The MYC family oncogenes (MYC, MYCN, and MYCL) encode transcription factors that regulate genes involved in a variety of fundamental cellular processes, including cell proliferation, metabolism, apoptosis, differentiation, stemness, and senescence in normal as well as neoplastic cells [1–3]. Recent findings suggest that MYC not only functions through cell-intrinsic mechanisms, but also plays an important role in communication with the microenvironment, including the immune system [4,5]. Deregulated expression of MYC family genes has been implicated in the development of over half of all human cancers, and often correlates with aggressive disease and poor prognosis [6,7]. This is commonly due to amplification or translocation of MYC family loci, as often observed in lymphoma, neuroblastoma, breast cancer, ovarian cancer, and lung cancer. Deregulated expression of MYC can also be caused by aberrant upstream signaling involving, e.g., RAS, PI3K, WNT, EGF, or mTOR pathways. In hematological malignancies, the most well-known example of MYC deregulation is the translocation of MYC into the immunoglobulin loci, which is an obligatory event in Burkitt´s lymphoma but also occurs at a lower frequency in other B-cell type lymphoma, leukemia, and myeloma [8,9]. MYC

translocation or amplification is quite rare in myeloid malignancies, however, gain of MYC can occur through trisomy of chromosome 8, and MYC expression is frequently deregulated as a consequence of the BCR/ABL activation and other translocation events in chronic myeloid leukemia (CML) and in acute myeloblastic leukemia (AML). As a consequence, MYC expression is linked to tumor progression and poor prognosis in different types of leukemias [10–14].

While aberrant MYC expression fuels excessive cell proliferation and tumorigenesis, it is simultaneously a potent trigger of apoptosis. During MYC-induced tumor development, events deactivating the apoptosis machinery, such as p53 mutation/loss or activation of BCL-2 family members, are therefore selected for. An example of this is the so-called double-hit B-cell lymphoma (DHL) harboring activating translocations for both MYC and BCL-2, which displays an exceedingly poor prognosis [15].

An alternative approach to target tumors with a defective apoptosis machinery exploits the concept of pro-senescence therapy [16–18]. Cellular senescence is defined as a state of irreversible cell cycle arrest, where cells do not respond to growth signals but remain metabolically active [19–21]. Alongside with apoptosis, senescence represents a major barrier against tumor development, but is also involved in normal processes such as aging, wound healing and embryonic development [22]. Senescence can be triggered by stress signals including DNA damage and oncogenic stress (so-called oncogene-induced senescence, OIS) and usually engages the p53/p21 and p16/pRb pathways [19–21,23]. Typical features of senescence include elevated senescence-associated β-galactosidase (SA-β-Gal) activity, increased cell size, and formation of senescence-associated heterochromatin foci containing trimethylated histone 3 at lysine 9 (H3K9me3). Furthermore, senescence is also characterized by secretion of a large number of chemokines and cytokines, defining the senescence-associated secretory phenotype (SASP) which modulates the immune surveillance of the senescent cells [19–21].

Like apoptosis, the senescence pathway requires to be inactivated or suppressed during tumor development, commonly through p53/p21 and/or the p16/pRb pathway impairment. The latter is controlled by cyclin-dependent kinases (CDKs), primarily CDK2 and CDK4/6, and inactivation of these CDKs have been shown to trigger senescence in tumor cells [24–28].

A large body of evidence also indicates that MYC plays an important role in suppressing senescence [26,27,29–35]. While MYC is an upstream regulator of CDK expression and/or activity, there is an interesting interplay between MYC and CDK2. We previously reported that MYC-mediated repression of RAS-induced senescence is dependent on CDK2 activity, and requires phosphorylation of MYC at Ser-62 by CDK2. In addition, depletion or pharmacological inhibition of CDK2 could restore RAS-induced senescence [26], suggesting a potentially useful strategy to target MYC in tumors, in particular those where the ability of MYC to induce apoptosis have been crippled.

Here, we utilized a previously established mouse model of AML driven by the concomitant overexpression of MYC and BCL-X_L [36] to investigate the potential of CDK2 inhibition for induction of senescence in AML cells and explore how that would affect tumor development. Among the available more selective CDK2 inhibitors, CVT313 and its analog CVT2584 [37] have shown good activity and selectivity in inhibiting CDK2 based on our previous work on senescence, where their activities did not overlap significantly with those of selective CDK1 and CDK9 inhibitors at active concentrations [25,26]. CVT2584 was chosen for this study due to its more optimal efficacy *in vivo* compared with CVT313, and we wanted to avoid pan-CDK inhibitors due to their broader range of activities, and their reported toxicity in patients [38].

Our results show that daily treatment with CVT2584 reduced the leukemic load in all analyzed tissues and significantly improved mice survival linked to the induction of cellar senescence. Taken together, our data provide a rationale for the treatment of MYC-driven neoplasia by exploiting CDK2 inhibition as a strategy to inhibit tumor development through promotion of senescence.

Materials and methods

Cell lines and mice

The human retroviral packaging cell line Phoenix-Eco (kindly provided by Dr. G. P. Nolan, Stanford University, CA, USA) was grown as described [39]. Female age-matched (6–8 weeks) inbred BALB/c and C57BL/6 mice were purchased from the animal facility at the Department of Microbiology, Tumor and Cell Biology, Karolinska Institutet. All mouse experiments were performed under the ethical guidelines of the Swedish Board of Agriculture and were approved by the animal ethics committee of North Stockholm.

Production of retroviral particles

Ten micrograms of the plasmids pMSCV-BCL-X_L-IRES-EGFP (enhanced green fluorescent protein) (BCL-X_L-GFP) and pMSCV-MYC-IRES-EYFP (enhanced yellow fluorescent protein) (MYC-YFP) expression vectors were used to transiently transfect the Phoenix-Eco packaging cell line using LipofectAMINE 2000 Reagent (11668019, Invitrogen). Supernatants containing recombinant viral particles were harvested 48 and 72 hours after transfection, passed through a 0.45 μm membrane, and kept in aliquots at −80°C until viral transduction.

Hematopoietic stem cell enrichment and retroviral transduction

Bone marrow was extracted from the *femur* and *tibia* of 10–12 week old BALB/c female mice 48 hours after intraperitoneal (i.p.) injection of 100 μl 5-fluorouracil (30 mg/ml) (Mayne Pharma Pic, Warwickshire, UK) to expand the stem cell compartment. Bone marrow cells were enriched for hematopoietic progenitors and stem cells (HSCs) by negative selection using the StemSep kit (13309, StemCell Technologies) according to the manufacturer's specifications. Cells were cultured for 24 hours in OPTIMEM (31985070, Invitrogen) supplemented with 10% FCS, 2 mM L-glutamine, 1 mM sodium pyruvate, 50 U/ml penicillin, 50 mg/ml streptomycin, 1% IL-6, 3% IL-3 and 3% SCF containing supernatants [40]. Next, HSCs were co-transduced by two rounds of spin infection with combinations of BCL-X_L-GFP and MYC-YFP retroviral particles in the presence of 10 mg/ml polybrene (TR-1003, Sigma-Aldrich). This procedure was repeated for three consecutive days and the cells were then cultured for an additional three days. The percentage of GFP and YFP positive cells was measured by flow cytometry prior to transplantation.

In vitro analysis of MYC/BCL-X_L transduced HSCs

1×10^5 cells were seeded, in triplicates, in the presence of 1 μM CVT2584 or in DMSO at day 0. Absolute cell numbers were counted in a Bürker chamber at 1, 3 and 5 days post-seeding. For measurement of SA-β-gal activity and apoptosis *in vitro*, see below.

Animal experiments, treatments and ex-vivo analyses

Transplantation was performed by tail vein injection of 1×10^6 cells into lethally irradiated (800 rad) syngeneic recipient BALB/c mice. Doxycycline (20 mg/ml, J01AA02, Merckle GmbH) was supplemented in the drinking water, and mice were kept in filter top cages and monitored for survival. In the case of the reintroduced MYC-YFP/BCL-X_L-GFP leukemic cell experiments, 3×10^5 cells were injected intravenously into sub-lethally irradiated (650 rad) C57BL/6 mice.

Transplanted BALB/c or C57BL/6 mice were treated on a daily basis *via* i.p. injection with vehicle DMSO, CVT2584 (generously provided by J. Zablocki, CV Therapeutics, Inc.) at 0.16 mg/kg body weight (bw), 1.6 mg/kg bw or 16 mg/kg bw. In some experiments, vehicle and CVT2584 were administered through an osmotic mini-pump (Alzet, Cupertino, CA, USA) transplanted intraperitoneally with a release rate of 2.5 mg/kg/hour. Doxorubicin (D2975000, Sigma-Aldrich) was administered via single i.p. injection at a concentration of 5 mg/kg bw. The treated mice were monitored daily for signs of disease by palpation as well as observation and were judged

as terminally ill when they displayed signs of paralysis in limbs or persistently hunched posture and slow movements. Mononuclear cell suspensions of spleen, liver, and bone marrow were obtained by straining tissues through nylon mesh cell strainers (352340, BD Biosciences). Portions of the spleen and liver tissues were fixed overnight (O/N) in 4% paraformaldehyde (PFA) in PBS, and further processed for paraffin embedding. The remaining spleen and liver tissues were embedded in OCT medium, snap-frozen, and stored at −80°C.

Flow cytometry analysis

Single-cell suspensions from spleen, femoral bone marrow and liver were incubated with monoclonal antibodies (MAb) against Gr1-APC (560599, BD Biosciences) and pacific blue-labeled anti-CD11b (clone M1/70.15). The latter MAb were prepared in our laboratory according to standard procedures. Biotinylated samples were then incubated with streptavidin-APC (554067, BD Biosciences) before being analyzed on a Cyan ADP flow cytometer (Beckman Coulter). EGFP and EYFP were detected using 510/21-nm and 550/30-nm band pass filters separated by a dichroic 525-nm mirror. Flow cytometric data were analyzed with FlowJo (Tree Star).

Histochemical detection of SA-β-gal activity

SA-β-gal activity was evaluated in splenic tissue of vehicle- and CVT2584-treated mice using Biovision's senescence detection kit (K320-250, Biovision) according to the manufacturer's specification. For *in vitro* analysis of MYC/BCL-X$_L$ transduced HSCs, SA-β-gal activity was monitored at day 5 after treatment. For quantification of SA-β-gal positive cells, 100 cells were counted, in three randomly selected fields, for each experimental condition. Statistical significance was calculated through a two-tailed unpaired students t-test. *p < 0.05, **p < 0.01.

Immunofluorescence staining

Five μm thick sections of formalin-fixed paraffin-embedded splenic tissues were blocked and permeabilized in PBS supplemented with 0.05% tween (PBS-T) and 3% BSA. Primary antibodies against Ki67 (GA626, Dako) and H3K9me3 (07–523, Millipore) as well as fluorophore-conjugated secondary antibodies AlexaFluor 488 and AlexaFluor 555 (A32731 and A32773, Invitrogen) were added in blocking solution, O/N, at 4°C. Extensive washing of the samples was performed between antibody incubations with PBS containing 0.1% triton X-100. The slides were mounted using Invitrogen antifade mounting medium containing DAPI (P36934, Thermoscientific). The samples were analyzed using an Axiovert 200M fluorescence microscope (Zeiss).

Protein analysis

Splenic tissue (200 mg) was ground in 400 μl of protein lysis buffer (1% NP-40, 0.1 M Tris pH 8, 150 mM NaCl, 5 mM EDTA, 2 μg/ml aprotinin) supplemented with a cocktail of protease and phosphatases inhibitors (5892970001 and 4906837001, Roche). The protein lysate was sonicated and centrifuged at 13,000 rpm for 10 minutes at 4°C. 50 μg of total protein was denatured in sample buffer for 10 minutes at 95°C, loaded onto a 4–12% Bis-Tris precast gel and run at 115 mA for 1 hour (NP0321BOX, Invitrogen). The gel was further transferred to a PVDF membrane using the iBlot dry system blotting (Invitrogen). The membrane was blocked in blocking buffer (PBS-T, 5% BSA) on a shaking platform for 30 minutes at RT, after which it was incubated with primary antibody O/N, with constant rotation/tilting at 4°C. The membranes were washed in PBS-T for 1 hour at RT, followed by incubation with a secondary-HRP-conjugated secondary antibody in blocking buffer as above, washed in PBS-T 3 times and developed with chemiluminescent HRP substrate. Antibodies used for immunoblotting were anti-p19[ARF] (ab80, Abcam), anti-p21[CIP1] (sc-397, Santa Cruz), anti-Rb (558385, BD Pharmingen), cyclin A1 (sc-239, Santa Cruz), anti-MYC (sc-764, Santa Cruz), phospho-Ser-62 MYC

(A300-206A, Bethyl Laboratories), anti-BCL-X$_L$ (2764S, Cell Signaling), anti-rabbit HRP-conjugated (ab97080, Abcam), anti-mouse HRP-conjugated (ab97046, Abcam).

Apoptosis assays

Apoptosis in splenic sections was assessed by using the *In Situ* Cell Death Detection Kit (11684795910, Roche), according to the manufacturer instructions (TUNEL assay). The stained sectioned were imaged and quantified using ImageJ software. Apoptosis in cell cultures was assessed using Annexin V-PE staining (559763, BD Biosciences), according to the manufacturer's instructions. Following annexin staining, the cells were analyzed using flow cytometry (FACSCalibur, BD Biosciences) and the percentage of apoptotic cells was calculated using CellQuest Pro software (BD biosciences).

Statistics

Quantifications of positive staining were performed using ImageJ. Statistical analysis was performed in GraphPad. Bar graphs are represented as mean with standard deviation. Statistical significance was determined by the Student t-test, ANOVA Brown-Forsythe (for multiple comparisons). Kaplan-Meier survival curves were analyzed using the Gehan-Breslow-Wilcoxon test for significance. $*P < 0.05$; $**P < 0.01$; $***P < 0.001$.

Results

Inhibition of CDK2 delays MYC/BCL-X$_L$-driven acute myeloblastic leukemia in vivo and improves survival

To determine whether pharmacological inhibition of CDK2 affects MYC/BCL-X$_L$-driven leukemia development *in vivo*, we used an AML model based on the transplantation of *MYC* and *BCL-X$_L$* expressing murine HSCs into lethally irradiated syngeneic host mice as described previously [36] and further outlined in Figure 1. Murine lineage-negative (Lin$^-$) HSCs were enriched from the bone marrow and transduced with replication-incompetent retroviral expression vectors

containing MYC and BCL-X$_L$ together with YFP and GFP, respectively. We first evaluated if CDK2 inhibition affected cell growth and senescence of MYC/BCL-X$_L$-transformed HSC cells in culture. MYC/BCL-X$_L$-transduced HSCs were treated with the selective CDK2 inhibitor CVT2584, which is an analog of CVT313 [37], or DMSO for 5 days. Treatment with CVT2584 resulted in a significant reduction in cell growth compared to DMSO (Figure 2(a)). SA-β-gal assay revealed a significant increase in cells positive for SA-β-gal activity compared to the control DMSO-treated MYC/BCL-X$_L$ HSCs at day 5 (Figure 2(b)). In contrast to the DNA-damaging agent ellipticine, exposure to CVT2584 did not induce apoptosis in MYC/BCL-X$_L$-transformed HSC cell cultures (Figures S1(a,b)), suggesting that CDK2 inhibition by CVT2584 inhibited proliferation and triggered senescence in MYC/BCL-X$_L$ transduced HSCs in culture.

Based on the results in cultured cells, we next determined whether CVT2584 inhibits MYC/BCL-X$_L$-driven leukemia development *in vivo*. MYC/BCL-X$_L$-transduced HSCs were transplanted into lethally irradiated syngeneic recipient BALB/c mice. The first signs of disease were observed 3 days after transplantation, as determined by the quantification of the
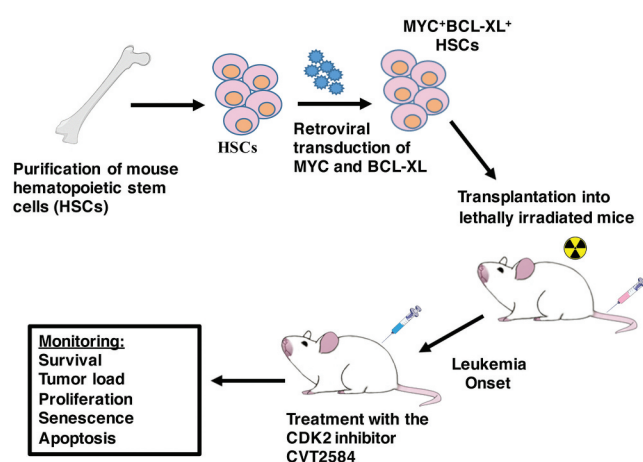

Figure 1. The MYC/BCL-X$_L$-driven acute myeloid leukemia model and outline of the experimental setup. Hematopoietic stem cells (HSC) purified from bone marrow cells of BALB/c mice are transduced with lentiviral vectors containing MYC and BCL-X$_L$ cDNA and then transplanted into lethally irradiated BALB/c mice. Upon disease onset mice are treated with the CDK2 inhibitor CVT-2584 or vehicle and monitored for survival, tumor load, and markers of senescence, proliferation and apoptosis.
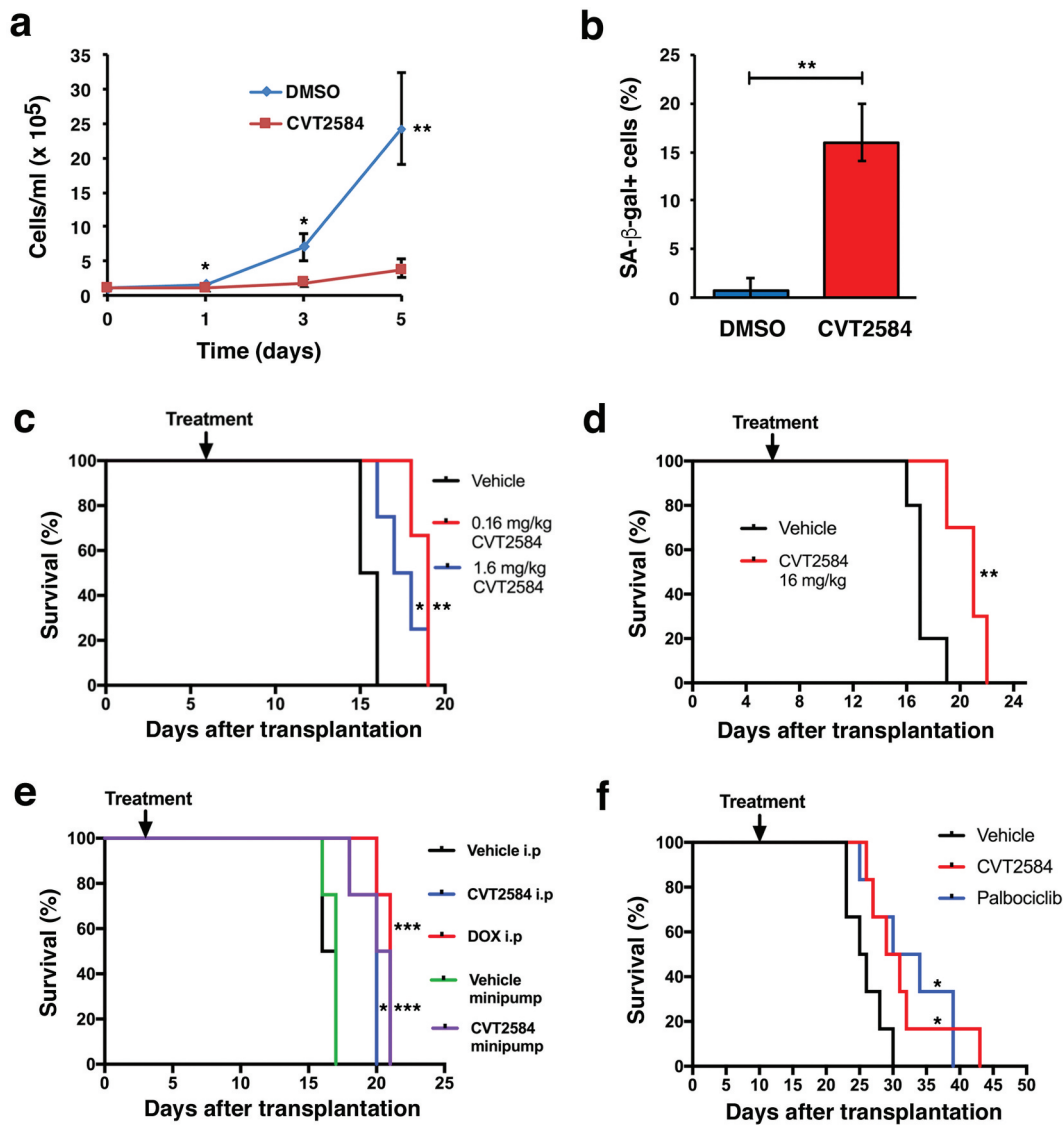
Figure 2. Pharmacological treatment with CDK2 inhibitor CVT2684 delays tumor development and improves overall survival of mice with MYC/BCL-X$_L$-induced leukemia. (a and b) CVT4584 treatment of MYC+BCL-X$_L$-transduced HSCs in culture induces growth arrest and senescence. (a) MYC/BCL-X$_L$-transduced HSCs in culture were treated with CVT2584 (1 μM) after which cell number was counted. (b) SA-β-Gal staining of MYC/BCL-X$_L$ HSCs in culture after CVT2584 treatment for 5 days. (c–f) Kaplan-Meier survival analysis of vehicle- and CVT2584-treated mice after transplantation with (c–e) HSCs over-expressing MYC and BCL-X$_L$ or (f) purified MYC/BCL-X$_L$ leukemic cells (c). The mice were treated from day 6 after transplantation with either 0.16 (blue, N = 4) or 1.6 mg/kg bw (red, N = 3) CVT2584 or vehicle (N = 2) via daily i.p. injections. Vehicle vs. 1.6 mg/kg bw CVT2584: p-value 0.0019, vehicle vs. 0.16 mg/kg bw CVT2584: p-value 0.0158. (d) The mice were treated from day 6 after transplantation with either 16 mg/kg bw CVT2584 (red) or vehicle (black) via daily i.p. injections. N = 10 for all. Vehicle vs. CVT2584: p-value 0.0001. (e) The mice were first treated with 0.16 mg/kg bw (day 3–5 after transplantation) and thereafter 16 mg/kg bw CVT2584 (blue) or vehicle (black) via daily i.p. injections or continuous administration of 2.5 mg/kg/hour CVT2584 (purple), 2.5 mg/kg/hour vehicle (green) via an osmotic mini-pump, or a single injection of (5 mg/kg bw) doxorubicin (DOX) (red). N = 4 for each cohort. Vehicle i.p. vs. DOX: p-value 0.004, vehicle i.p. vs. CVT2584 i.p.: p-value 0.0116, vehicle mini-pump vs. CVT2584 mini-pump: p-value 0.0084. (f) The mice were injected with purified MYC/BCL-X$_L$ leukemic cells, and then treated from day 10 after transplantation with either 16 mg/kg bw CVT2584 (red) or vehicle (black) via daily i.p. injections or 100 mg/kg bw palbociclib (red) via oral gavage. N = 8 for all. Vehicle vs. CVT2584: p-value 0.0372, vehicle vs. palbociclib: p-value 0.012.

presence of leukemic blasts in histological smears from peripheral blood (Figure S1(c)). The mice were treated with CVT2584 (0.16 mg/kg bw or 1.6 mg/kg bw) or DMSO vehicle, which were administered daily via intraperitoneal (i.p.) injections starting from day 6 after transplantation. The vehicle-treated

hosts rapidly displayed signs of disease such as ruffled fur, wasting, and slow movements that developed into hind limb paralysis, in line with our previous observations [36]. The median survival for DMSO-treated mice was 15.5 days after transplantation (Figure 2 (c)). The progression of the disease was significantly delayed in mice exposed to either 0.16 or 1.6 mg/kg bw of CVT2584, and the median survival of the mice was prolonged with 2 and 3 days to 17.5 and 19 days post-transplantation, respectively, in comparison with vehicle-treated mice, correlating with the escalating dose of CVT2584 (Figure 2(c)). Next, we aimed to improve the survival of the mice by increasing the concentration of CVT2584 to 16 mg/kg/bw and evaluated the effect on overall survival. The median survival for vehicle-treated animals was 17 days, which was prolonged to 21 days with CVT2584 (16 mg/kg bw) (Figure 2(d)), providing a median survival benefit of 4 days. We next tested whether an earlier treatment and a different modality of administration could increase the therapeutic benefit of CVT2584. In order to avoid potential interference with the bone marrow reconstitution process, the mice were initially given i.p. injections with the lower dose of 0.16 mg/kg bw of CVT2584 or vehicle from 3 days after transplantation. The dose was then increased to 16 mg/kg bw of CVT2584 and maintained for the daily i.p. treatment. The median survival for vehicle-and CVT2584-treated animals was now 17 and 20 days, respectively (Figure 2(e)). Considering the rapid turnover of CVT2584 *in vivo*, estimated half-life 1.2 hours in serum (pers. communication J. Zablocki), we decided to try to maintain active drug concentration through application of osmotic mini-pumps (miniature infusion systems for continuous dosing), which were implanted into the animals and delivered a fixed dose of CVT2584 (2.5 mg/kg/hour) or vehicle at a constant rate. The mice receiving CTV2584 through mini-pumps showed a marginally improved median survival to 20.5 days, compared to 20 days when CVT2584 was administered i.p., improving the overall survival by 4 days compared with vehicle (16.5 days) (Figure 2(e)). We also compared the efficiency of the CVT2584 with the well-established anti-cancer compound doxorubicin (DOX), a chemotherapeutic agent commonly used in a wide range of cancers, including leukemia. DOX-treated mice showed a median

survival of 21 days after transplantation, i.e. a similar improvement of survival as the administration of CVT2584 (20.5 days) (Figure 2(e)).

Considering the aggressiveness of the disease, we proceeded to titrate the numbers of transplanted cells in hopes of slowing down the kinetics of tumor development and further allowing for a wider window of opportunity for the treatment. We, therefore, switched from a pool of transduced HSCs to defined numbers of purified MYC/BCL-X_L leukemic cells. MYC/BCL-X_L-overexpressing leukemic cells were harvested from the spleens of moribund mice and reintroduced into sub-lethally irradiated recipient mice. After injection of 3×10^5 AML cells, leukemic blast cells were readily detectable in blood smears at day 7, compared to day 3 in the HSCs-based model (data not shown). Treatment with vehicle or CVT2584 (16 mg/kg bw) administrated daily via i.p injections started at day 10. As a reference compound, the FDA-approved selective CDK4/6 inhibitor palbociclib [41] was administered (100 mg/kg bw) via oral gavage for 10 days (5 days treatment, 2 days rest, 5 days treatment in total). The median survival recorded was 25 days, 30 days and 32 days after transplantation for DMSO, CVT2584, and palbociclib, respectively (Figure 2(f)). Therefore, although there was a significant extension in the survival following CVT2584 treatment (as compared with vehicle) by 5 days (Figure 2(f)), the median survival was not significantly improved in comparison to CVT2584 treatment in the previous experiments (Figure 2(c–e)). The effect of palbociclib on survival was not significantly enhanced in comparison to CVT2584 despite administered at a sixfold higher concentration. Notably, body weights of CVT2584-treated mice remained relatively stable throughout the experiment, while the body weights of vehicle-treated animals declined steadily from day 18 onwards as a result of AML development (Figure S1(d)). This suggests that CVT2584 at the given concentration (16 mg/kg bw) was well tolerated.

Taken together, these data suggest that pharmacological targeting of CDK2 by CVT2584 leads to

delayed MYC/BCL-X$_L$-driven leukemia development and a moderate yet significant improvement of survival of the mice.

Pharmacological inhibition of CDK2 in vivo results in significant reduction in tumor load

We set out to determine whether pharmacological CDK2 inhibition by CVT2584 affected the expansion and accumulation of the MYC/BCL-X$_L$-overexpressing leukemic population. Necropsy of CVT2584- and vehicle-treated AML-bearing mice showed that leukemic cells disseminated throughout the hematopoietic tissues with extensive involvement of spleen, bone marrow and infiltration of the liver. To quantitate the effect on tumor load, spleen, bone marrow and liver cell suspensions from CVT2584- and vehicle-treated animals were stained for CD11b$^+$/Gr1$^+$ AML cells [36] and analyzed by flow cytometry. The AML cell population was significantly reduced in the spleen and liver of CVT25854-treated compared with vehicle-treated animals (Figure 3(a–c)). A similar trend was also observed in the bone marrow of CVT25854-treated animals, although this did not reach significance.

Similarly, there was a significant reduction in the weight of the spleens in the CVT2584-treated cohort (mean weight: 440 mg) compared to vehicle-treated mice (mean weight: 680 mg) (Figure 3 (d)). Further, flow cytometry analysis of YFP +/GFP+ cells, i.e. cells expressing MYC and BCL-X, in the bone marrow and spleen of mice transplanted with purified MYC/BCL-X leukemic cells according to the experiment in Figure 2(f), also showed a significant reduction in the leukemic cell population following CVT2584 treatment Figure 3(e,f), which is in line with the results presented in Figure 3(a–c). However, hematoxylin/eosin staining revealed no overt differences in spleen morphology between vehicle- and CVT2584-treated AML-bearing animals (Figure S1(e)).

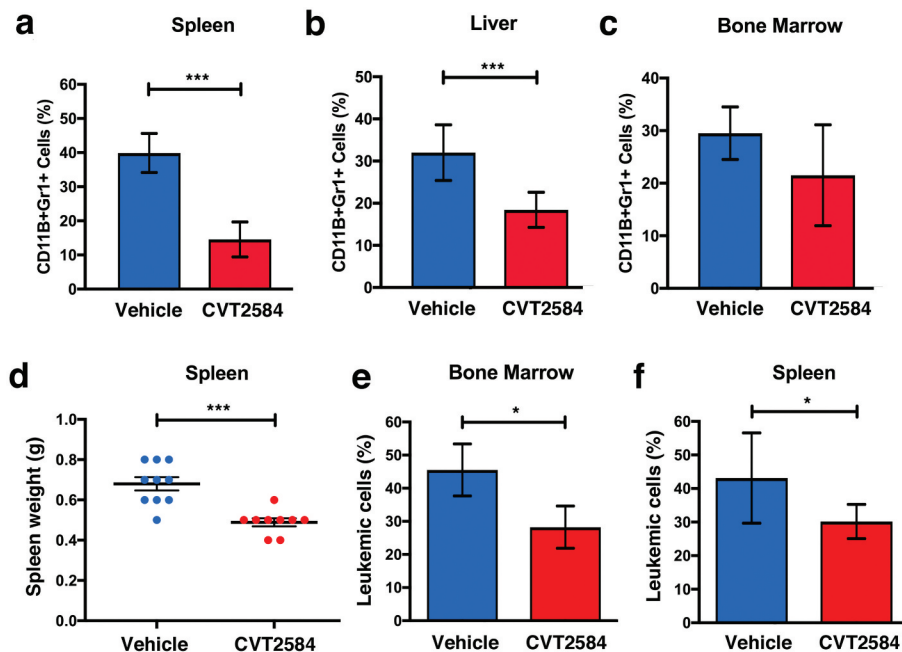$_{LL}$Figure 2(f Figure 3(eFigure 3(a–c)

Figure 3. Treatment with CDK2 inhibitor CVT2684 results in a reduction of the leukemic tumor load. (a–c) Flow cytometry analysis of CD11b$^+$Gr1$^+$ AML cell populations isolated from (a) spleen, (b) liver and (c) bone marrow, from vehicle- (N = 8) or CVT2584-treated (16 mg/kg bw, N = 7) mice (harvested at the end point). (d) Spleen weights of CVT2584- (16 mg/kg bw) or vehicle-treated AML-bearing animals (N = 10 in each group) at the time of sacrifice. This experiment corresponds to Figure 2(d). (e, f) Flow cytometry analysis of YFP$^+$/GFP$^+$(i.e. MYC/BCL-X$_L$) leukemic cell population in (e) bone marrow and (f) spleen of mice at the endpoint after CVT2584 (16 mg/kg bw) and vehicle treatment. N = 8 in each group. These mice were transplanted with purified MYC/BCL-X$_L$ leukemic cells as in Figure 2(f).

Collectively, these results suggest that pharmacological inhibition of CDK2 activity reduces the expansion of the MYC/BCL-X_L-driven leukemic population.

Inhibition of CDK2 reduces proliferation in leukemic cells invading the spleen in MYC/BCL-X_L mice

To evaluate whether the pharmacological inhibition of CDK2 affected proliferation, senescence, or apoptosis in MYC/BCL-X_L–induced AML cells *in vivo*, splenic tissue from CVT2584- and vehicle-treated mice were stained with markers representative of these states. First, we co-immunostained for the proliferation marker Ki67 and histone H3 phosphorylated at Ser 10 (P-H3S10), which is a marker of cells in mitosis [42]. A significant decrease in Ki67$^+$ as well as P-H3S10$^+$ cells was observed in spleen samples from CVT2584-treated compared to vehicle-treated animals (Figure 4(a,b)), as quantified in Figure 4(d,e). In agreement with these results, immunoblot analysis of cyclin A expression, which occurs in S- and G2 phases of the cell cycle, was notably reduced in all CVT2584-treated compared to vehicle-treated animals (Figure 4(f)). Taken together, these results are indicative of reduced leukemic cell proliferation in response to CDK2 inhibition.

Immunoblot analysis further showed that the protein levels of MYC and BCL-X_L were unchanged in all analyzed animals independent of CVT2584 dose relative to vehicle (Figure 4(f)). We have previously reported that CDK2 mediates phosphorylation of MYC at Ser-62, and that this phosphorylation is important for suppression of senescence by MYC [26]. To evaluate whether CDK2 inhibition reduced MYC Ser-62 phosphorylation *in vivo*, the spleen protein lysates were probed with antibodies recognizing MYC phosphorylated at Ser-62. In agreement with our previous report [26], reduced MYC Ser-62 phosphorylation was observed in CVT2584-treated compared with vehicle-treated animals, both at lower and higher doses of CVT2584 (Figure 4(f)), supporting the notion that CDK2 regulates MYC phosphorylation *in vivo*.

Inhibition of CDK2 induces senescence in leukemic cells invading the spleen in MYC/BCL-X_L mice

To inquiry whether the reduced cell proliferation observed in these specimens was due to the induction of cellular senescence, spleen sections were scored for SA-β-gal activity. Although samples from both CVT2584- and vehicle-treated mice showed a certain degree of positivity, the SA-β-gal staining was significantly increased in spleens from CVT2584-treated mice (Figure 5(a)), as quantitated in Figure 5(e). We also examined the presence of senescence-associated heterochromatin foci (SAHF), using an antibody directed against H3K9me3. Immunofluorescence staining of spleen tissue from CVT2584-treated mice showed a strong increase in SAHF formation compared to the vehicle-treated mice (Figure 5(b,f)). To investigate an additional marker of senescence, immunohistochemical staining for p19^{ARF} was performed. Nuclear p19^{ARF}-positive cells were readily detected in sections of CVT2584-treated animals but found virtually absent in the analyzed specimens from vehicle-treated animals (Figure 5(c,g)). In addition, immunoblot analysis showed increased p19^{ARF} protein levels as well as elevated levels of p21^{CIP1,} another marker of senescence, upon CDK2 inhibition compared to vehicle-treated animals (Figure 5(i)). In addition, since pRb is a CDK2 substrate as well as a senescence regulator, we analyzed changes in Rb phosphorylation status. Immunoblot analysis demonstrated an increase in the faster migrating hypophosphorylated active form of Rb in spleen of CVT2584-treated animals (Figure 5(i)), with the strongest signal deriving from hosts receiving higher concentration of CVT2584.

Both CVT2584- and vehicle-treated animals showed very few apoptotic cells, as examined by TUNEL staining (Figure 5(d,h)). In sharp contrast, control tissue obtained from untreated mice transplanted with HSCs transduced with MYC and RAS
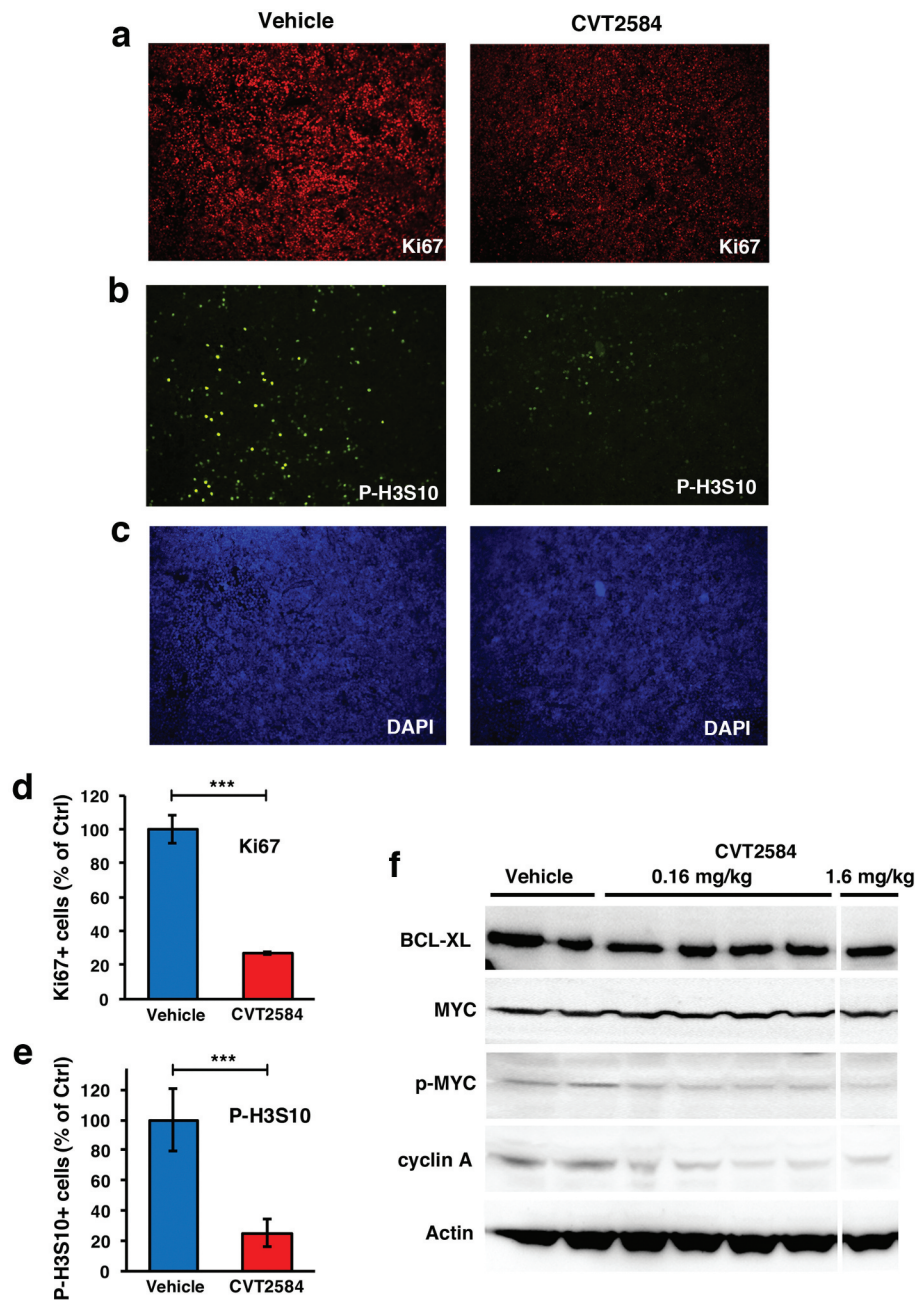
Figure 4. Inhibition of CDK2 by CVT2584 reduces the proliferation rates of the leukemic cells and reduces MYC Ser-62 phosphorylation in spleen tissue. Representative images of (a) Ki67 (red), (b) phospho(P)-H3S10 (green) and (c) DAPI (blue) immunofluorescence analysis of spleen tissues from vehicle- and CVT2584-treated (16 mg/kg bw) MYC/BCL-X$_L$ mice as indicated. 5X magnification. (d, e) Quantification of (d) Ki67 and (e) P-H3S10 stainings. (f) Immunoblot analysis of indicated proteins isolated from spleens from AML-bearing mice treated with vehicle or CVT2584 at indicated concentrations.

in the absence of BCL-X$_L$ showed abundant TUNEL staining (Figure 5(d,h)).

In summary, the above results suggest that pharmacological inhibition of CDK2 by CVT2584 reduced leukemic cell proliferation and induced cellular senescence, but did not trigger apoptosis, in spleen tissue from MYC/BCL-X$_L$ AML-bearing mice. Further, reduced phosphorylation of two

CDK2 substrates, pRb, and MYC, in AML-infiltrated spleen tissue confirms CDK2-inhibitory CVT2584 activity *in vivo* at applied concentrations.

Discussion

Here we utilized the MYC/BCL-X$_L$ AML mouse model [36], where MYC-induced apoptosis is blocked
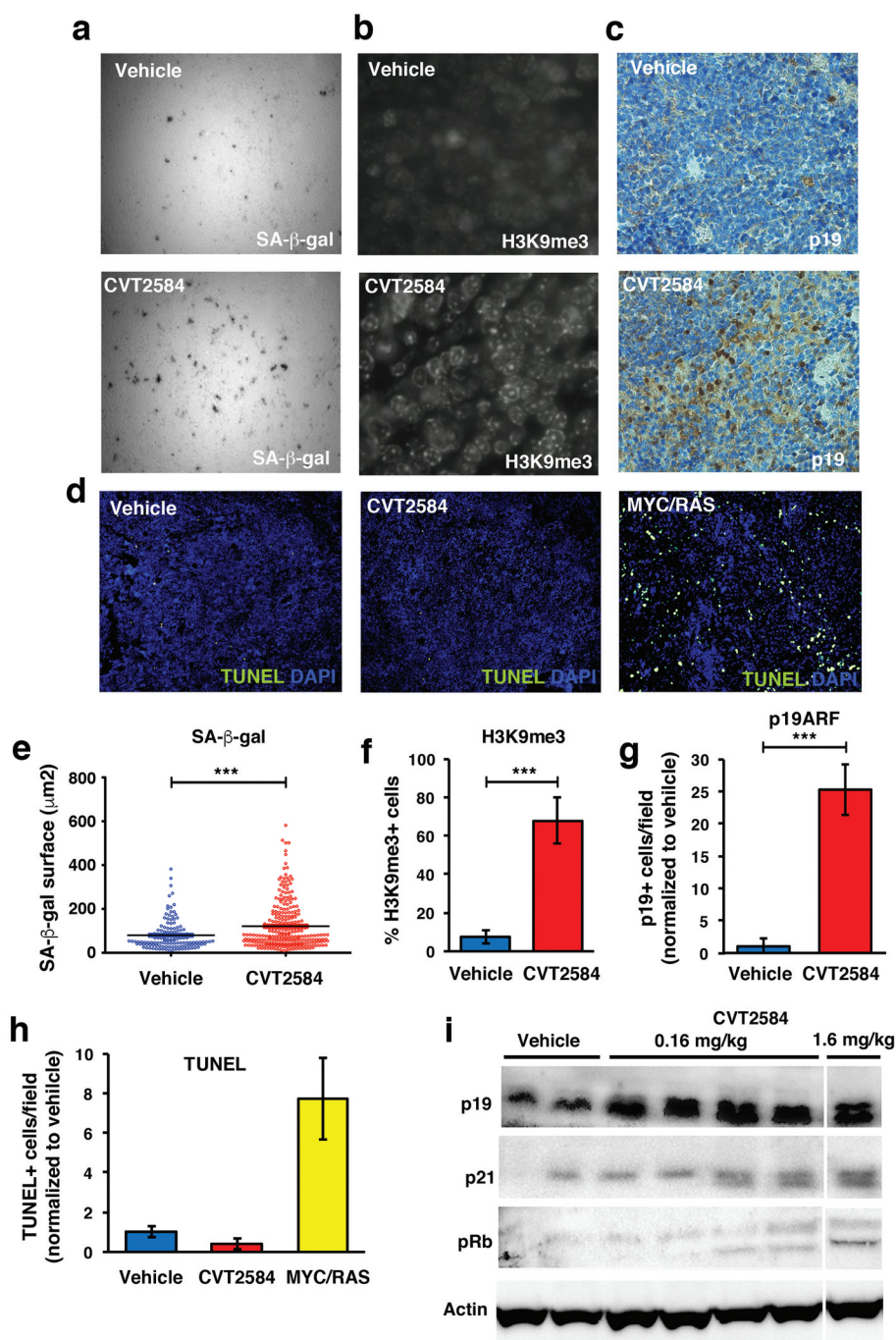
Figure 5. Inhibition of CDK2 by CVT2584 induces senescence in leukemic cells in spleen tissue. (a–d) Analysis of senescence markers in spleen samples from CVT2584- (16 mg/kg bw) and vehicle-treated AML-bearing mice. (a) SA-β-gal staining of fresh frozen spleen samples. 20X magnification. (b–d) Staining of PFA-fixed spleen samples. (b) SAHFs. Immunofluorescence staining using antibodies against H3K9me3. 60X magnification. (c) Immunohistochemical staining of p19 expression using anti-p19 antibodies. 40X magnification. (d) Apoptosis. TUNEL (green) and DAPI (blue) staining. 5X magnification. (e–h) Quantification of (e) SA-β⁻gal positive areas, (f) percentage of H3K9me3⁺ cells, (g) p19⁺ cells per field and (h) TUNEL⁺ cells per field, from the experiments in (a–d), respectively. (i) Immunoblot analysis of indicated proteins isolated from spleens from AML-bearing mice treated with vehicle or CVT2584 at indicated concentrations.

by BCL-X$_L$, to explore the potential of CDK2 as a promising druggable target for the potential induction of senescence as an alternative strategy to combat MYC-driven tumors. This was based on previous findings on the interplay between MYC and CDK2 in senescence regulation [25,26].

Prior to the *in vivo* studies, we showed that CVT2584 led to a robust senescence induction in purified MYC/BCL-X$_L$ AML cells *ex vivo* (Figure 2 (a,b)). A series of *in vivo* experiments were then performed to corroborate these results *in vivo*. Administration of CVT2584 led to a significant reduction in leukemic tumor load in all affected tissues at the endpoint of the experiment compared with vehicle. While vehicle-treated animals died from leukemia within 16–17 days post-injection of MYC/BCL-X$_L$-expressing HSCs, CVT2584-treatment significantly improved mice survival with additional 3–4 days (Figure 2(c,e)). A similar response was also observed after treatment with the conventional anti-cancer topoisomerase inhibitor doxorubicin, which is similar to daunorubicin, used in human AML treatment. A drawback with doxorubicin and other topoisomerase inhibitors is that they cause DNA damage, while selective targeting of CDK2, which is a non-essential gene, is likely to cause less severe side effects in a clinical setting. The FDA-approved CDK4/6 inhibitor palbociclib, which was used as a reference, did not show a significant difference in efficiency compared with CVT2584, despite being used at a sixfold higher concentration (Figure 2(f)).

At the biological and molecular levels, our study corroborates a clear induction of senescence following treatment with CVT2584, as determined by upregulation of the senescence markers SA-β-gal, H3K9me3-containing SAHFs, p19^{ARF} and p21^{CIP1}, as well as reduced expression of the proliferation markers Ki67, cyclin A and phospho-H3S10 (Figures 4 and 5). In addition, exposure to CVT2584 led to decreased levels of phosphorylation of pRb and MYC at Ser-62, both of which are reported substrates for CDK2 as well as senescence regulators [26,43], thereby confirming that CVT2584 indeed inhibits CDK2 *in vivo* at the given doses. Concomitantly, the absence of activation of the apoptotic cascade suggests that inhibition of CDK2 favored a senescence response via the p53/p19^{ARF}/p21^{CIP1} and pRb pathways. This is consistent with our previous report from rodent fibroblasts, leukemia cell cultures and EμMyc mice [25,26], and shows that CDK2 inhibition induces

a similar senescence program in MYC/BCL-X$_L$-driven AML *in vivo*.

Using a MLL-AF9–NRAS^{G12D}-driven leukemia mouse model, Baker and colleagues showed that the pan-CDK inhibitor dinaciclib was a potent inducer of apoptosis and significantly prolonged survival of these mice [44]. Tumors with MLL translocations are dependent on transcription elongation, which render them sensitive to CDK9 inhibition. While CDK9 was the suggested key target for dinaciclib in this case, dinaciclib, however, also inhibits CDK1, CDK2, and CDK5 at similar concentrations as CDK9, so the involvement of these CDKs in response to this drug cannot be ruled out. Nevertheless, the study highlights the potential of CDK inhibitors as promising treatment for hematological malignancies.

In light of the results presented in this report, it may seem surprising that the overall survival improvement, albeit significant, was quite moderate, extending the life of experimental mice of 3–5 days in different settings. However, one should bear in mind the very aggressive nature of this AML model, leading to a median survival of 15–17 days, which is comparable to what has been reported from MLL/ENL+NRAS- and MLL/AF9 + NRAS-driven leukemia transplantation systems (2–3 weeks). Of note, administration of chemotherapy or targeted therapies (such as BET or HDAC inhibitors) to mice carrying any of these MLL-driven AMLs was reported to provide the same magnitude of survival benefits as those observed after CVT2584 treatment in this study [45–47]. Another consideration is the rapid turnover of CVT2584 *in vivo* (1.2 hours, data not shown), which limits the efficacy of the treatment. We tried to solve this issue by continuous supply of CVT2584 via implantation of osmotic mini-pumps, but the maximum concentration of the compound that can be loaded in these devices represents a limiting factor. A further limitation with our experimental model is that the reconstitution of the bone marrow following the transplantation of the transduced HSCs requires lethal irradiation of recipient mice, which puts constraints on the harshness of the treatment due to the vulnerability of the mice. We, therefore, tried

to circumvent this restriction by transplanting a smaller amount of purified leukemic cells into sub-lethally irradiated mice, which slowed down the progression of the disease but nevertheless did not substantially improve survival after CVT2584 treatment compared with the other experimental setups (Figure 2(f)).

It is also worth noting that the CVT2584-treated animals displayed a lower tumor load than the vehicle-treated animals at the experimental endpoint. The rapid onset and progression of the disease is likely causing organ failure in the spleen, liver and bone marrow of the hosts. We speculate that a sharp decline in functionality of these organs may cause difficulties to cope with the accumulation of senescent tumor cells, including the production of SASP factors, thereby limiting the survival benefit of the treatment. This relates to the subject of safety with pro-senescence therapy, and warrants further investigation.

Our results also raise the question whether a subpopulation of leukemic cells escaped the effects of CVT2584, eventually leading to death of these mice. In a study by Campaner and colleagues, genetic depletion of CDK2 resulted in a delay in the development of Eμ-myc-driven lymphomas, which was overcome by acquired mutations in p53 and/or other senescence effector genes [25]. A similar escape mechanism seems less likely to occur in our AML model due to the short time required for mice to reach an ethical endpoint. Another explanation is that CDK2 inhibition is not sufficient for a complete senescence response. It may be necessary to combine CDK2 inhibition with molecules targeting other senescence regulators such as CDK4, p53, SKP2, or PTEN. This may be one of the reasons why increasing CVT2584 concentrations beyond 1.6 mg/kg did not improve the outcome, although more trivial explanations such as decreased solubility at higher concentrations are also conceivable. Another possibility is that CDK2 inhibition may trigger epigenetic changes that will compensate for loss of CDK2 activity. Recent studies suggest that tumor cells escaping senescence can reprogram into stem cell–like cells that are intrin-

sically less responsive to therapy [48]. Furthermore, SASP factors secreted by senescent cells can play an adverse role by promoting angiogenesis and suppression of the immune system depending on the context [49]. To prevent this scenario, different ways of eliminating senescent tumor cells are under development. For instance, so-called senolytic drugs, such as the BCL2/BCL-X$_L$ inhibitor Navitoclax, have been shown to clear senescent cancer cells through apoptosis [50]. Such drugs could potentially be used in combination with CDK2 inhibitors for cancer treatment in the future.

The present study adds to previous studies from our lab as well as other groups suggesting that CDK2 is an interesting alternative target for cancer therapy, in particular in MYC-driven tumors such as MYCN-amplified neuroblastoma, MYC-driven B lymphoma, MYC/MYCN-driven medulloblastoma and triple-negative breast cancer [25–27,51–54]. Other candidates for CDK2 therapy are breast and ovarian cancer with amplification and overexpression of its activating partner cyclin E, but also prostate and colorectal cancer, glioblastoma, Ewing's sarcoma and hematopoietic malignancies, including diffuse large B-cell lymphoma and AML have been suggested [54–56]. Of note, CDK2 has been implicated in drug resistance development to CDK4/6 inhibition in breast cancer [57], and CDK2 targeting could therefore be a treatment option for such patients.

In summary, the present work demonstrates that pharmacological CDK2 inhibitor CVT2584 significantly delays MYC/BCL-X$_L$-driven leukemia through induction of cellular senescence. Together with other reports, this work suggests that CDK2 is a promising target for cancer therapy, in particular for MYC-driven tumors, warranting the development of new, more potent, and selective CDK2 inhibitors in the future.

Disclosure statement

Funding

ORCID

Matteo Bocci http://orcid.org/0000-0002-8774-0006
Lars-Gunnar Larsson http://orcid.org/0000-0001-6914-3147

References

[1] Conacci-Sorrell M, McFerrin L, Eisenman RN. An overview of MYC and its interactome. Cold Spring Harb Perspect Med. 2014;4:a014357.

[2] Kress TR, Sabo A, Amati B. MYC: connecting selective transcriptional control to global RNA production. Nat Rev Cancer. 2015;15:593–607.

[3] Stine ZE, Walton ZE, Altman BJ, et al. MYC, metabolism, and cancer. Cancer Discov. 2015;5:1024–1039.

[4] Casey SC, Tong L, Li Y, et al. MYC regulates the antitumor immune response through CD47 and PD-L1. Science. 2016;352:227–231.

[5] Kortlever RM, Sodir NM, Wilson CH, et al. Myc cooperates with Ras by programming inflammation and immune suppression. Cell. 2017;171:1301–1315 e1314.

[6] Gabay M, Li Y, Felsher DW. MYC activation is a hallmark of cancer initiation and maintenance. Cold Spring Harb Perspect Med. 2014;4(6):a014241.

[7] Kalkat M, De Melo J, Hickman KA, et al. MYC deregulation in primary human cancers. Genes (Basel). 2017;8(6):151.

[8] Delgado MD, Leon J. Myc roles in hematopoiesis and leukemia. Genes Cancer. 2010;1:605–616.

[9] Schick M, Habringer S, Nilsson JA, et al. Pathogenesis and therapeutic targeting of aberrant MYC expression in haematological cancers. Br J Haematol. 2017;179:724–738.

[10] Abraham SA, Hopcroft LE, Carrick E, et al. Dual targeting of p53 and c-MYC selectively eliminates leukaemic stem cells. Nature. 2016;534:341–346.

[11] Jones L, Wei G, Sevcikova S, et al. Gain of MYC underlies recurrent trisomy of the MYC chromosome in acute promyelocytic leukemia. J Exp Med. 2010;207:2581–2594.

[12] Ohanian M, Rozovski U, Kanagal-Shamanna R, et al. MYC protein expression is an important prognostic factor in acute myeloid leukemia. Leuk Lymphoma. 2019;60:37–48.

[13] Schreiner S, Birke M, Garcia-Cuellar MP, et al. MLL-ENL causes a reversible and myc-dependent block of myelomonocytic cell differentiation. Cancer Res. 2001;61:6480–6486.

[14] Yun S, Sharma R, Chan O, et al. Prognostic significance of MYC oncoprotein expression on survival outcome in patients with acute myeloid leukemia with myelodysplasia related changes (AML-MRC). Leuk Res. 2019;84:106194.

[15] Bisso A, Sabo A, Amati B. MYC in germinal center-derived lymphomas: mechanisms and therapeutic opportunities. Immunol Rev. 2019;288:178–197.

[16] Acosta JC, Gil J. Senescence: a new weapon for cancer therapy. Trends Cell Biol. 2012;22:211–219.

[17] Larsson LG. Cellular senescence–a barrier against tumor development? Semin Cancer Biol. 2011;21:347–348.

[18] Nardella C, Clohessy JG, Alimonti A, et al. Pro-senescence therapy for cancer treatment. Nat Rev Cancer. 2011;11:503–511.

[19] Campisi J, d'Adda Di Fagagna F. Cellular senescence: when bad things happen to good cells. Nat Rev Mol Cell Biol. 2007;8:729–740.

[20] Gorgoulis V, Adams PD, Alimonti A, et al. Cellular senescence: defining a path forward. Cell. 2019;179:813–827.

[21] Hernandez-Segura A, Nehme J, Demaria M. Hallmarks of cellular senescence. Trends Cell Biol. 2018;28:436–453.

[22] Munoz-Espin D, Serrano M. Cellular senescence: from physiology to pathology. Nat Rev Mol Cell Biol. 2014;15:482–496.

[23] Serrano M, Lin AW, McCurrach ME, et al. Oncogenic ras provokes premature cell senescence associated with accumulation of p53 and p16INK4a. Cell. 1997;88:593–602.

[24] Anders L, Ke N, Hydbring P, et al. A systematic screen for CDK4/6 substrates links FOXM1 phosphorylation to senescence suppression in cancer cells. Cancer Cell. 2011;20:620–634.

[25] Campaner S, Doni M, Hydbring P, et al. Cdk2 suppresses cellular senescence induced by the c-myc oncogene. Nat Cell Biol. 2010;12(sup):54–59.

[26] Hydbring P, Bahram F, Su Y, et al. Phosphorylation by Cdk2 is required for Myc to repress Ras-induced senescence in cotransformation. Proc Natl Acad Sci U S A. 2010;107:58–63.

[27] Hydbring P, Castell A, Larsson LG. MYC modulation around the CDK2/p27/SKP2 axis. Genes (Basel). 2017;8:174.

[28] Rader J, Russell MR, Hart LS, et al. Dual CDK4/CDK6 inhibition induces cell-cycle arrest and senescence in neuroblastoma. Clin Cancer Res. 2013;19:6173–6182.

[29] Juan J, Muraguchi T, Iezza G, et al. Diminished WNT -> beta-catenin -> c-MYC signaling is a barrier for malignant progression of BRAFV600E-induced lung tumors. Genes Dev. 2014;28:561–575.

[30] Mallette FA, Gaumont-Leclerc MF, Huot G, et al. Myc down-regulation as a mechanism to activate the Rb pathway in STAT5A-induced senescence. J Biol Chem. 2007;282:34938–34944.

[31] Swartling FJ, Grimmer MR, Hackett CS, et al. Pleiotropic role for MYCN in medulloblastoma. Genes Dev. 2010;24:1059–1072.

[32] Tabor V, Bocci M, Alikhani N, et al. MYC synergizes with activated BRAFV600E in mouse lung tumor development by suppressing senescence. Cancer Res. 2014;74:4222–4229.

[33] van Riggelen J, Muller J, Otto T, et al. The interaction between Myc and Miz1 is required to antagonize TGFbeta-dependent autocrine signaling during lymphoma formation and maintenance. Genes Dev. 2010;24:1281–1294.

[34] Wu CH, van Riggelen J, Yetil A, et al. Cellular senescence is an important mechanism of tumor regression upon c-Myc inactivation. Proc Natl Acad Sci U S A. 2007;104:13028–13033.

[35] Zhuang D, Mannava S, Grachtchouk V, et al. C-MYC overexpression is required for continuous suppression of oncogene-induced senescence in melanoma cells. Oncogene. 2008;27:6623–6634.

[36] Hogstrand K, Hejll E, Sander B, et al. Inhibition of the intrinsic but not the extrinsic apoptosis pathway accelerates and drives MYC-driven tumorigenesis towards acute myeloid leukemia. PLoS One. 2012;7:e31366.

[37] Brooks EE, Gray NS, Joly A, et al. CVT-313, a specific and potent inhibitor of CDK2 that prevents neointimal proliferation. J Biol Chem. 1997;272:29207–29211.

[38] Whittaker SR, Mallinger A, Workman P, et al. Inhibitors of cyclin-dependent kinases as cancer therapeutics. Pharmacol Ther. 2017;173:83–105.

[39] Nyakeriga AM, Djerbi M, Malinowski MM, et al. Simultaneous expression and detection of multiple retroviral constructs in haematopoietic cells after bone marrow transplantation. Scand J Immunol. 2005;61:545–550.

[40] Karasuyama H, Melchers F. Establishment of mouse cell lines which constitutively secrete large quantities of interleukin 2, 3, 4 or 5, using modified cDNA expression vectors. Eur J Immunol. 1988;18:97–104.

[41] Fry DW, Harvey PJ, Keller PR, et al. Specific inhibition of cyclin-dependent kinase 4/6 by PD 0332991 and associated antitumor activity in human tumor xenografts. Mol Cancer Ther. 2004;3:1427–1438.

[42] Van Hooser A, Goodrich DW, Allis CD, et al. Histone H3 phosphorylation is required for the initiation, but not maintenance, of mammalian chromosome condensation. J Cell Sci. 1998;111(Pt 23):3497–3506.

[43] Akiyama T, Ohuchi T, Sumida S, et al. Phosphorylation of the retinoblastoma protein by cdk2. Proc Natl Acad Sci U S A. 1992;89:7900–7904.

[44] Baker A, Gregory GP, Verbrugge I, et al. The CDK9 Inhibitor Dinaciclib Exerts Potent Apoptotic and Antitumor Effects in Preclinical Models of MLL-Rearranged Acute Myeloid Leukemia. Cancer Res. 2016;76:1158–1169.

[45] Bots M, Verbrugge I, Martin BP, et al. Differentiation therapy for the treatment of t(8;21) acute myeloid leukemia using histone deacetylase inhibitors. Blood. 2014;123:1341–1352.

[46] Zuber J, Radtke I, Pardee TS, et al. Mouse models of human AML accurately predict chemotherapy response. Genes Dev. 2009;23:877–889.

[47] Zuber J, Shi J, Wang E, et al. RNAi screen identifies Brd4 as a therapeutic target in acute myeloid leukaemia. Nature. 2011;478:524–528.

[48] Milanovic M, Fan DNY, Belenki D, et al. Senescence-associated reprogramming promotes cancer stemness. Nature. 2018;553:96–100.

[49] Campisi J. Aging, cellular senescence, and cancer. Annu Rev Physiol. 2013;75:685–705.

[50] Zhu Y, Tchkonia T, Fuhrmann-Stroigg H, et al. Identification of a novel senolytic agent, navitoclax, targeting the Bcl-2 family of anti-apoptotic factors. Aging Cell. 2016;15:428–435.

[51] Bolin S, Borgenvik A, Persson CU, et al. Combined BET bromodomain and CDK2 inhibition in MYC-driven medulloblastoma. Oncogene. 2018;37:2850–2862.

[52] Horiuchi D, Huskey NE, Kusdra L, et al. Chemical-genetic analysis of cyclin dependent kinase 2 function reveals an important role in cellular transformation by multiple oncogenic pathways. Proc Natl Acad Sci U S A. 2012;109:E1019–1027.

[53] Molenaar JJ, Ebus ME, Geerts D, et al. Inactivation of CDK2 is synthetically lethal to MYCN over-expressing cancer cells. Proc Natl Acad Sci U S A. 2009;106:12968–12973.

[54] Tadesse S, Anshabo AT, Portman N, et al. Targeting CDK2 in cancer: challenges and opportunities for therapy. Drug Discov Today. 2020;25:406–413.

[55] Musa J, Cidre-Aranaz F, Aynaud MM, et al. Cooperation of cancer drivers with regulatory germline variants shapes clinical outcomes. Nat Commun. 2019;10:4128.

[56] Ying M, Shao X, Jing H, et al. Ubiquitin-dependent degradation of CDK2 drives the therapeutic differentiation of AML by targeting PRDX2. Blood. 2018;131:2698–2711.

[57] Herrera-Abreu MT, Palafox M, Asghar U, et al. Early adaptation and acquired resistance to CDK4/6 inhibition in estrogen receptor-positive breast cancer. Cancer Res. 2016;76:2301–2313.